

# Excited state quantum phase transition and Loschmidt echo spectrum in a spinor Bose-Einstein condensate

Zhen-Xia Niu<sup>1</sup> and Qian Wang<sup>1,2\*</sup>

<sup>1</sup>*Department of Physics, Zhejiang Normal University, Jinhua 321004, China*

<sup>2</sup>*CAMTP-Center for Applied Mathematics and Theoretical Physics,  
University of Maribor, Mladinska 3, SI-2000, Maribor, Slovenia*

(Dated: March 22, 2024)

Identifying dynamical signatures of excited state quantum phase transitions (ESQPTs) in experimentally realizable quantum many-body systems is helpful for understanding the dynamical effects of ESQPTs. In such systems, the highly controllable spinor Bose-Einstein condensates (BECs) offer an exceptional platform to study ESQPTs. In this work, we investigate the dynamical characteristics of the ESQPT in spin-1 BEC by means of the Loschmidt echo spectrum. The Loschmidt echo spectrum is an extension of the well-known Loschmidt echo and defined as the overlaps between the evolved state and the excited states of the initial Hamiltonian. We show that both the time evolved and long time averaged Loschmidt echo spectrum undergo a remarkable change as the system passes through the critical point of the ESQPT. Moreover, the particular behavior exhibited by the Loschmidt echo spectrum at the critical point stand as a dynamical detector for probing the ESQPT. We further demonstrate how to capture the features of the ESQPT by using the energy distribution associated with the Loschmidt echo spectrum for time evolved and long time averaged cases, respectively. Our findings contribute to a further verification of the usefulness of the Loschmidt echo spectrum for witnessing various quantum phase transitions in many-body systems and provide a new way to experimentally examine the dynamical consequences of ESQPTs.

## I. INTRODUCTION

Understanding the notion of excited state quantum phase transitions (ESQPTs) in quantum many-body systems has attracted a lot of interest in recent years [1–6]. As a generalization of the ground state quantum phase transition [7] to excited states, ESQPTs exist in a wide range of quantum many-body systems, including the interacting boson model [2, 8–10], molecular bending transitions [11–13], the kicked and coupled top models [14–17], the Kerr-nonlinear oscillator [18, 19], the spinor Bose-Einstein condensates (BECs) [20–23], the Lipkin-Meskov-Glick (LMG) model [2, 24–29], as well as the Dicke and Rabi models [30–34]. A prominent signature of ESQPTs is the non-analyticities in the density of states (DOS) and the energy that leads to the divergence in the DOS is defined as the ESQPT critical energy.

There is a vast amount of theoretical studies on the effects of ESQPTs. It was known that ESQPTs can strongly affect the quantum dynamics after a quench [30, 35–42], localize the eigenstates [28, 29], accelerate the time evolution of the system [43–45], and create the Schrödinger cat states [46]. ESQPTs are also closely connected with the onset of chaos [15, 47–49] and different types of dynamical quantum phase transitions [50, 51]. The particular role played by the ESQPTs in the thermalization process of isolated quantum systems has also been revealed recently [52, 53]. Moreover, the endeavour to explore the order parameters of ESQPTs [6, 21, 32, 38, 54] provides further insights into the excited state phases.

The experimental observations of ESQPTs are mainly focused on the singularities of the DOS in molecular bending transitions [11, 12] and microwave Dirac billiards [55]. To experimentally investigate the dynamical consequences of an ESQPT, the highly controllable experimental platforms are required. A suitable platform to explore the dynamical signatures of ESQPTs is the spinor BECs [56, 57], as they can be realized and controlled by the current experimental techniques [58–63] and they exhibit ESQPTs in excited states [20–23]. Even though signatures of the ground state quantum phase transition and associated dynamical features in spinor BECs have been theoretically analyzed [56, 57, 64–67] and testified in various experiments [63, 68–74], only a few recent studies are concerning about the characteristics of ESQPTs [21, 22].

In this work, we investigate the dynamical signatures of ESQPT in the spin-1 BEC using the Loschmidt echo spectrum [75]. The Loschmidt echo spectrum extends the conventional concept of the Loschmidt echo beyond the ground state and is defined as the overlaps between the evolved state and the excited states. As the dynamics in a quantum system is governed by its whole energy spectrum, one can expect that the Loschmidt echo spectrum will provide more dynamical characteristics of the system. The usefulness of the Loschmidt echo spectrum in studying of the dynamical quantum phase transitions has been verified [75], while here we examine its ability to characterize the ESQPT.

The ESQPT in the spin-1 BEC is signified by the logarithmic divergence of the DOS and it can lead to an abrupt change in the structure of eigenstates. The analysis of the classical limit of the system shows that the onset of ESQPT can be considered as a consequence of the saddle point in its classical counterpart. We show

---

\* [qwang@zjnu.edu.cn](mailto:qwang@zjnu.edu.cn)

that the underlying ESQPT exhibits strong impact on the time evolution of the Loschmidt echo spectrum. Both the existence and different phases of the ESQPT can be reliably identified by the properties of the Loschmidt echo spectrum and associated energy distribution. We further display how the ESQPT manifests itself in the long time averaged Loschmidt echo spectrum and associated energy distribution. The aim of the present work is to access the signatures of ESQPT from both time evolved and long time averaged behaviors of the Loschmidt echo spectrum, as well as to provide further evidence of the validity of the Loschmidt echo spectrum for diagnosing various phase transitions in quantum many-body systems.

The rest of the article is structured as follows. In Sec. II, we introduce the considered physical system and its classical limit, discuss the basic features of the ESQPT. Our main results are presented in Sec. III, where we report the properties of the Loschmidt echo spectrum and associated energy distribution, and reveal their connection with the ESQPT for time evolved and long time averaged cases, respectively. Finally, we summarize our results and conclude in Sec. IV.

## II. QUANTUM SYSTEM

We consider the spin-1 BEC, which describes  $N$  mutually interacting atoms with three hyperfine spin states  $m = 0, \pm 1$  and can be experimentally realized by  $^{87}\text{Rb}$  and  $^{23}\text{Na}$  atoms [56, 57]. Using the single-mode approximation [56] which decouples the spin and spatial degrees of freedom, the Hamiltonian of the system can be written as [56, 57]

$$\frac{\hat{H}}{|c|} = \frac{\text{sign}(c)}{N} \left[ \hat{a}_0^\dagger \hat{a}_1 \hat{a}_{-1} + \hat{a}_1^\dagger \hat{a}_{-1} \hat{a}_0^2 + \hat{N}_0(\hat{N}_1 + \hat{N}_{-1}) + \frac{1}{2}(\hat{N}_1 - \hat{N}_{-1})^2 \right] + \kappa(\hat{N}_1 + \hat{N}_{-1}). \quad (1)$$

Here,  $\hat{a}_m(\hat{a}_m^\dagger)$  with  $m = 0, \pm 1$  are the bosonic annihilation (creation) operators for spin state  $m$ ,  $\hat{N}_m = \hat{a}_m^\dagger \hat{a}_m$  denote the atom number operators and satisfy  $\sum_m \hat{N}_m = \hat{N}$ . The parameter  $c$  refers the strength of the inter-spin interaction with  $c < 0$  ( $c > 0$ ) for ferromagnetic (antiferromagnetic) BEC [56], while  $\kappa \equiv q/|c|$  represents the effective quadratic Zeeman shift and can take both positive and negative values by means of microwave dressing [60, 62].

The Hamiltonian (1) conserves the magnetization  $\hat{\mathcal{M}}_z = \hat{N}_1 - \hat{N}_{-1}$  and parity  $(-1)^{\hat{N}_0}$  [21]. In this work, we restrict our analysis to the even parity subspace with  $\mathcal{M}_z = 0$ , thus the Hilbert space has dimension  $\mathcal{D}_{\mathcal{H}} = N/2 + 1$ . Moreover, we only consider the ferromagnetic spinor BEC with  $c < 0$  and  $\kappa \geq 0$ . However, we would like to point out that it is straightforward to generalize our studies to the cases of antiferromagnetic spinor condensate,  $\mathcal{M}_z \neq 0$  and  $\kappa < 0$ .

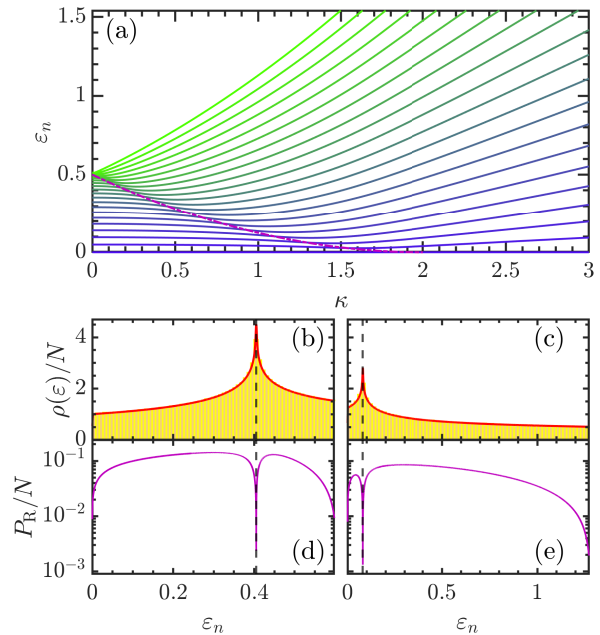


FIG. 1. (a): Rescaled energy levels  $\varepsilon_n = (E_n - E_0)/N$  as a function of  $\kappa$  with  $N = 40$ . The purple dot-dashed line denotes the critical energy of ESQPT, as given in Eq. (5). (b)-(c): Normalized density of states  $\rho(\varepsilon)/N$  for  $\kappa = 0.2$  (b) and  $\kappa = 1.2$  (c) with  $N = 10000$ . The red solid lines are the analytical results, see Eq. (6). (d)-(e): Rescaled participation ratio  $P_R/N$  as a function of  $\varepsilon_n$  for the same values of  $\kappa$  as in panels (b) and (c) with  $N = 10000$ . The vertical dashed lines in panels (b)-(e) represent the critical energy of the ESQPT obtained from Eq. (5).

For our considered case, it is known that the system exhibits a ground state quantum phase transition at the critical point  $\kappa_c = 2$ , which divides the broken-axisymmetry phase with  $\kappa < 2$  from the polar phase with  $\kappa > 2$  [57, 65–69]. In addition, the existence of ESQPTs and the relevant signatures and applications in spinor BECs have also been investigated in recent works [20–23].

### A. Excited state quantum phase transitions

ESQPTs are signified by the clustering of the eigenlevels, which results in the singularities in the DOS [2, 5]. To illustrate the ESQPT in the spinor BEC, we analyze the spectrum of Hamiltonian (1) as a function of control parameter  $\kappa$ . In Fig. 1(a), we show how the rescaled excitation energies,  $\varepsilon_n = (E_n - E_0)/N$ , evolve with increasing  $\kappa$ . Here,  $E_n$  denotes  $n$ th eigenenergy of  $\hat{H}$  and  $E_0$  is its ground state energy. One can see that, the excited eigenlevels exhibit an obvious cluster along the dot-dashed line, which marks the critical energy of the ESQPT, denoted by  $\varepsilon_c$ . We further observe that the critical energy  $\varepsilon_c$  decreases with increasing  $\kappa$  and moves to-

wards to the known ground state QPT as  $\kappa$  approaches 2. By utilizing the mean-field approximation, the explicit dependence of the critical energy  $\varepsilon_c$  on the control parameter  $\kappa$  can be obtained analytically [see Eq. (5) below]. As a consequence of the eigenlevels cluster, the DOS,  $\rho(\varepsilon) = \sum_n \delta(\varepsilon - \varepsilon_n)$ , shows a sharp peak at  $\varepsilon_c$  for the cases of  $\kappa < 2$ , as visualized in Figs. 1(b) and 1(c). In the  $N \rightarrow \infty$  limit, the peak in the DOS turns into a logarithmic divergence, which makes up a prominent signature of the ESQPT.

The emergence of the ESQPT is also closely connected with the localization of the eigenstates, namely, the eigenstates in the neighborhood of  $\varepsilon_c$  are the highly localized states [28, 29]. The degree of localization of the eigenstates  $|\psi_n\rangle$  for a given basis  $\{|\alpha_k\rangle\}$ , is measured by the participation ratio  $P_R = 1/|c_k^{(n)}|^4$ , where  $c_k^{(n)} = \langle \alpha_k | \psi_n \rangle$ . For the spin-1 BEC, the basis consists of the Fock states  $|\alpha_k\rangle = |N_{-1}, N_0, N_1\rangle$ . The extended state has larger value of  $P_R$ , while a small  $P_R$  indicates the localized state. Figs. 1(d) and 1(e) plot the rescaled participation ratio as a function of  $\varepsilon_n$  for different control parameters. A sharp dip in the behavior of  $P_R$  at  $\varepsilon_n \sim \varepsilon_c$  is clearly visible. The appearance of dip in  $P_R$  means the eigenstate at the critical energy is localized in the Fock basis.

## B. Classical limit

More insights into the characters of the ESQPT can be obtained by analyzing the properties of the stationary points in the corresponding classical system. To derive the classical counterpart of the Hamiltonian (1), we first note that in the classical limit with  $N \rightarrow \infty$ , the spin states are described by the coherent states [21, 23, 76]

$$|\xi\rangle = \frac{1}{\sqrt{N!}} \left( \xi_{-1} a_{-1}^\dagger + \xi_0 a_0^\dagger + \xi_1 a_1^\dagger \right) |0\rangle, \quad (2)$$

where  $|0\rangle$  is the vacuum state,  $\xi_m = \sqrt{N_m} e^{i\varphi_m}$  with  $\varphi_m \in [-\pi, \pi)$  and  $\sum_m N_m = N$ . Then by using the relation  $\langle \xi | a_m | \xi \rangle = \xi_m$ , it is straightforward to find that the classical Hamiltonian with  $N_{-1} = N_1$  is given by [21, 56, 77]

$$H_{cl} = \lim_{N \rightarrow \infty} \frac{\langle \xi | \hat{H} | \xi \rangle}{N} = \kappa(1 - \zeta_0) - 2\zeta_0(1 - \zeta_0) \cos^2 \varphi, \quad (3)$$

where  $\zeta_0 = N_0/N$  and  $\varphi = \varphi_0 - (\varphi_1 + \varphi_{-1})/2$ . The classical equations of motion are, therefore, given by

$$\begin{aligned} \dot{\varphi} &= \frac{\partial H_{cl}}{\partial \zeta_0} = -\kappa - 2(1 - 2\zeta_0) \cos^2 \varphi, \\ \dot{\zeta}_0 &= -\frac{\partial H_{cl}}{\partial \varphi} = -2\zeta_0(1 - \zeta_0) \sin(2\varphi), \end{aligned} \quad (4)$$

with the constrained condition  $d(\varphi_1 - \varphi_{-1})/dt = 0$ .

By setting  $\dot{\varphi} = \dot{\zeta}_0 = 0$ , one can find that the classical system (3) has three fixed points when  $\kappa < 2$ .

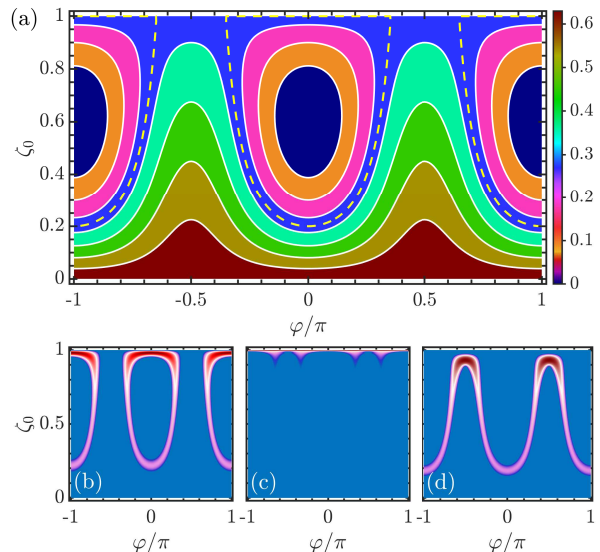


FIG. 2. (a): Energy contours of the classical Hamiltonian (3) in the phase space. The yellow dashed line denotes the separatrix given by Eq. (5). (b)-(d): Rescaled Husimi distributions,  $\mathcal{Q}(\zeta_0, \varphi) = Q(\zeta_0, \varphi)/Q_{max}(\zeta_0, \varphi)$  for  $\varepsilon_n = 0.2909$  (b),  $\varepsilon_n = \varepsilon_c = 0.32$  (c), and  $\varepsilon_n = 0.347$  (d) with  $N = 300$ . Other parameter:  $\kappa = 0.4$ .

They are two stable points  $\{\cos \varphi, \zeta_0\} = \{\pm 1, (2 + \kappa)/4\}$  with the minimal energy of the classical system  $\mathcal{E}_{min} = -(\kappa - 2)^2/8$ , and a saddle point at  $\zeta_0 = 1$  with energy  $\mathcal{E}_s = 0$ . In Fig. 2(a), we plot the energy contours in phase space for the classical system. We observe two different structures in the energy surface. The change in the structure of the classical energy surface indicates the presence of the separatrix in the classical dynamics. The equation of separatrix in Fig. 2(a) is determined by the energy difference  $\mathcal{E}_s - \mathcal{E}_{min}$ , which also corresponds to the critical energy of the ESQPT,

$$\varepsilon_c = \frac{(\kappa - 2)^2}{8}, \quad (5)$$

with  $0 < \kappa < 2$ . This result has been plotted as the purple dot-dashed line in Fig. 1(a).

The agreement between the separatrix and the energy of the ESQPT implies that the logarithmic divergence in the DOS is a consequence of the saddle point in the underlying classical counterpart. To see this, we consider the semiclassical approximation of the DOS in the subspace with  $N_{-1} = N_1$  [21],

$$\frac{\rho_{cl}(\varepsilon)}{N} = \frac{1}{(2\pi)^3} \int \mathcal{D}\xi \delta(\zeta_{-1} - \zeta_1) \delta(\varepsilon - H_{cl}), \quad (6)$$

where  $\mathcal{D}\xi = \prod_m d\zeta_m d\varphi_m \delta(\sum_k \zeta_k - 1)$ . Here, we would like to point out that  $\rho_{cl}(\varepsilon)$  provides the smooth component in the Gutzwiller trace formula [78]. The integral in above equation can be carried out by employing the property of the delta-function and the final results

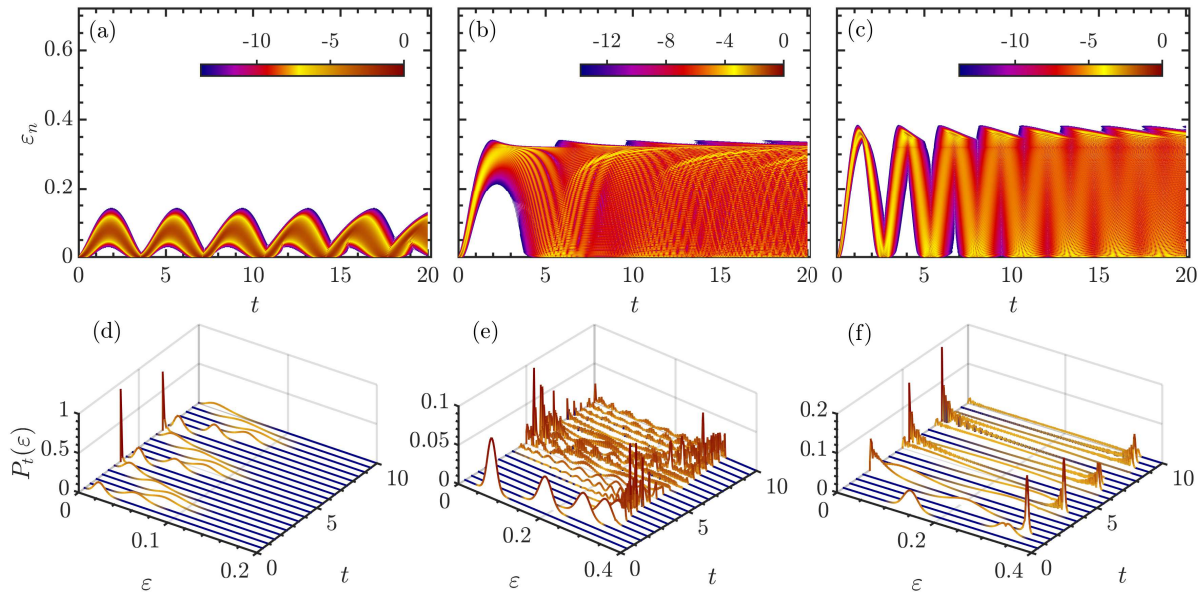


FIG. 3. (a)-(c) Color plot of the Loschmidt echo spectrum (in logarithmic scale) as a function of  $t$  and  $\varepsilon_n$  for  $\delta\kappa = 0.4$  (a),  $\delta\kappa = \delta\kappa_c = 0.8$  (b), and  $\delta\kappa = 1.2$  (c). In each panel, the white regions denote  $L_n(t) = 0$ . (d)-(f) Evolving of the energy distribution  $P_t(\varepsilon)$  [cf. Eq. (10)] as a function of  $t$  for the same values of  $\delta\kappa$  as in panels (a)-(c). Other parameters:  $N = 1000$ ,  $\kappa_i = 0.4$  and  $\delta\kappa_c = 0.8$  [see Eq. (8)].

for different control parameters  $\kappa$  are plotted as the red solid lines in Figs. 1(b) and 1(c). We see an excellent agreement between the numerical data and the behavior of  $\rho_{cl}(\varepsilon)/N$ . In particular,  $\rho_{cl}(\varepsilon)/N$  shows an obvious singularity at the critical energy of the ESQPT.

The existence of the saddle point in the classical system also explains the localization at the critical energy of the ESQPT. To see this, we consider the localization behavior of an eigenstate  $|\varepsilon_n\rangle$  in the classical phase space, which can be visualized by the Husimi distribution [79]

$$Q(\zeta_0, \varphi) = |\langle \varepsilon_n | \xi \rangle|^2. \quad (7)$$

It is known that the Husimi distribution  $Q(\zeta_0, \varphi)$  offers the quasiprobability distribution of  $|\varepsilon_n\rangle$  in the classical phase space with canonical variables  $(\zeta_0, \varphi)$ .

Figs. 2(b)-(d) plot the Husimi distribution for the eigenstates with energy below, at, and above the critical energy of the ESQPT. For the eigenstate with the critical energy of the ESQPT [Fig. 2(c)], the Husimi distribution displays a highly concentrated feature in the phase space. By contrast, the Husimi distribution for the eigenstates with energy below and above the ESQPT is extended in the phase space, as seen in Figs. 2(b) and 2(d), respectively. The behaviors of the Husimi distribution for different eigenstates are consistent with the variation of the participation ratio with the eigenenergy.

### III. LOSCHMIDT ECHO SPECTRUM AND ESQPT

In the rest of the article, we analyze the dynamical signatures of the ESQPT by means of the Loschmidt echo spectrum. To this end, we assume the system is initially prepared in the ground state  $\rho(0) = |\psi_0\rangle\langle\psi_0|$  of  $\hat{H}_i$  with  $\kappa = \kappa_i$ . Then, at  $t = 0$ , we suddenly change the control parameter to a new value  $\kappa = \kappa_i + \delta\kappa$  and focus on the dynamics of the system governed by the postquench Hamiltonian  $\hat{H}_f$ . As changing of the control parameter  $\kappa$  leads to the varying energy in the system, one can drive the system crossing different phases of the ESQPT by tuning the value of  $\delta\kappa$ . The critical quench strength, denoted by  $\delta\kappa_c$ , is defined as the one that takes the system to the critical energy of the ESQPT. Employing the mean-field approximation, one can find  $\delta\kappa_c$  is given by

$$\delta\kappa_c = 1 - \frac{\kappa_i}{2}, \quad (8)$$

where  $0 \leq \kappa_i \leq 2$ .

After quench, the state of the system at time  $t$  is  $\rho(t) = e^{-i\hat{H}_f t} \rho(0) e^{i\hat{H}_f t}$ . To extract the dynamical signatures of the ESQPT from  $\rho(t)$ , we use the Loschmidt echo spectrum [75]

$$L_n(t) = \text{Tr}[\rho_n \rho(t)] = \left| \sum_{\alpha} \langle \psi_n | \alpha \rangle \langle \alpha | \psi_0 \rangle e^{-iE_{\alpha} t} \right|^2, \quad (9)$$



where  $\rho_n = |\psi_n\rangle\langle\psi_n|$  is the  $n$ th eigenstate of  $\hat{H}_i$  with associated energy  $E_n$  and  $|\alpha\rangle$  is the  $\alpha$ th eigenstate of the postquench Hamiltonian  $\hat{H}_f$  with the corresponding eigenenergy  $E_\alpha$ , so that  $\hat{H}_f|\alpha\rangle = E_\alpha|\alpha\rangle$ .

The Loschmidt echo spectrum measures how the time evolved state spreads in the eigenstates of the initial Hamiltonian and its ability to probe the dynamical quantum phase transitions in quantum many-body systems has been investigated in a very recent work [75]. Since the ESQPT involves the whole energy spectrum of the system, we would expect that more dynamical signatures of the ESQPT can be revealed by the Loschmidt echo spectrum. Notice that the zero component of the Loschmidt echo spectrum,  $L_0$ , is the well-known survival probability, which has been widely used as a dynamical detector of ESQPTs [28–30, 39–43, 80].

Figs. 3(a)-(c) demonstrate how the Loschmidt echo spectrum evolves as a function of  $t$  for different quench strength  $\delta\kappa$  with the system size  $N = 1000$  and  $\kappa_i = 0.4$ , which determines  $\delta\kappa_c = 0.8$ . For the case with  $\delta\kappa < \delta\kappa_c$ , as illustrated in Fig. 3(a), the small quench strength can only scatter the quenched state into the low excited states of the initial Hamiltonian. As a consequence, the Loschmidt echo spectrum is highly concentrated in the low  $H_i$  eigenenergies, irrespective of the time. Moreover, small  $\delta\kappa$  value also leads to the revival of the initial state, which results in the regular oscillations in  $t$  of the Loschmidt echo spectrum. With increasing  $\delta\kappa$ , more excited states are involved and the number of excited states contributing to the Loschmidt echo spectrum increases. Once the critical quench  $\delta\kappa_c = 0.8$  is reached, the Loschmidt echo spectrum is quickly spreading out in a larger number of excited eigenenergies and shows a complex dependence on the time, as seen in Fig. 3(b). The fast spread of the Loschmidt echo spectrum at the critical quench can be considered as a result of the saddle point in the corresponding classical system, which gives rise to the dynamical instability in the quantum system [44, 45, 81–84]. As  $\delta\kappa$  increases further, such as  $\delta\kappa = 1.2$  case shown in Fig. 3(c), the evolution of the Loschmidt echo is initially regular followed by irregular oscillations and is also distributed in a wider range of excited eigenenergies. The regular behavior in the evolved Loschmidt echo spectrum is a consequence of the periodic trajectories in the underlying classical dynamics, while the long time irregular oscillations are due to the quantum interference effect on the evolution of the Loschmidt echo spectrum.

### A. Energy distribution of the evolved state

The dynamical features observed in Figs. 3(a)-(c) are more visible in Figs. 3(d)-(f), where we plot the time evolution of the energy distribution of the evolved state weighted by components  $L_n(t)$ ,

$$P_t(\varepsilon) = \sum_n L_n(t)\delta(\varepsilon - \varepsilon_n). \quad (10)$$

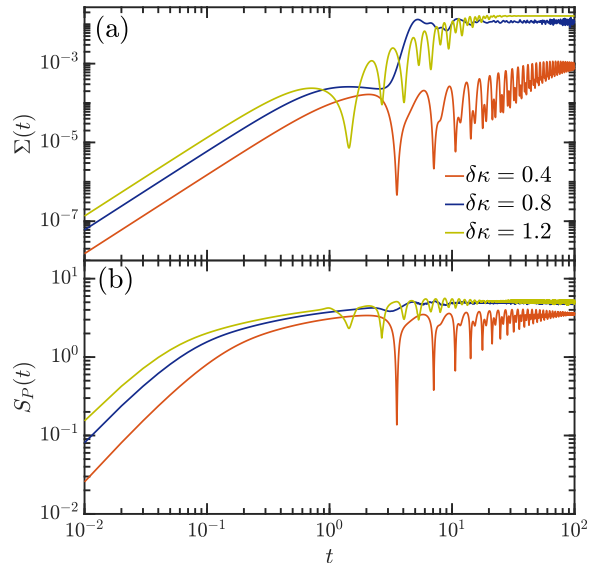


FIG. 4. (a)  $\Sigma(t)$  as a function of  $t$  for several quench strengths  $\delta\kappa$ . (b) Time evolution of the energy distribution entropy  $S_P(t)$  for different values of  $\delta\kappa$ . Other parameters:  $N = 1000$ ,  $\kappa_i = 0.4$  and  $\delta\kappa_c = 0.8$  [see Eq. (8)].

It can be considered as the vertical cutting version of the evolved  $L_n(t)$  at a fixed time and satisfies  $\int d\varepsilon P_t(\varepsilon) = 1$ . We see that the evolution of  $P_t(\varepsilon)$  shows obvious difference between two phases of the ESQPT. Hence, different phases of the ESQPT can be distinguished by the distinct behaviors in the evolved  $P_t(\varepsilon)$  for  $\delta\kappa < \delta\kappa_c$  and  $\delta\kappa > \delta\kappa_c$ , respectively. In addition, the singular behavior of  $P_t(\varepsilon)$  at the critical quench stands as a faithful figure of merit for diagnosing the presence of the ESQPT.

A main feature exhibited by  $P_t(\varepsilon)$  is the different degrees of extension over the excited eigenenergies, which can be quantified by the variation of  $P_t(\varepsilon)$  with the definition given by

$$\Sigma(t) = \int d\varepsilon P_t(\varepsilon)[\varepsilon - \langle\varepsilon\rangle]^2, \quad (11)$$

where  $\langle\varepsilon\rangle = \int d\varepsilon P_t(\varepsilon)\varepsilon$  is the averaging of  $\varepsilon$ .

Fig. 4(a) plots the variation of  $\Sigma(t)$  with increasing  $t$  for three different quench strengths, which are below, at, and above the critical quench strength. Overall, the initial growth of  $\Sigma(t)$  is followed by a small fluctuation around the saturation value, regardless of the strength of the quench. However, the way of  $\Sigma(t)$  growth is strongly depended on the quench strength. For  $\delta\kappa$  below the critical value,  $\Sigma(t)$  increases with larger oscillations and takes a long time to reach its saturation value with small oscillations. On the other hand, even though the growth of  $\Sigma(t)$  still shows many oscillations for  $\delta\kappa > \delta\kappa_c$  case, it saturates to a larger saturation value at a short time scale. At the critical quench  $\delta\kappa = \delta\kappa_c$ ,  $\Sigma(t)$  undergoes a fast growth which then quickly saturates to its saturation value with tiny fluctuations. We further note that

the saturation values of  $\Sigma(t)$  for  $\delta\kappa \geq \delta\kappa_c$  are almost independent of the quench strength.

These properties of  $\Sigma(t)$  suggest that the underlying ESQPT leaves an imprint in the dynamics of quenched system. The dynamics of  $\Sigma(t)$  can be used as a dynamical method to identify different phases of an ESQPT. Moreover, the existence of the ESQPT can be efficiently signified by the rapid growth behavior in  $\Sigma(t)$ .

Figs. 3(d)-(f) also demonstrate that the complexity of the evolved  $P_t(\varepsilon)$  is strongly depended on the quench strength. To measure the complexity of  $P_t(\varepsilon)$ , we study the entropy of  $P_t(\varepsilon)$ :

$$S_P(t) = - \int d\varepsilon P_t(\varepsilon) \ln P_t(\varepsilon). \quad (12)$$

It varies in the interval  $S_P(t) \in [0, \ln \Delta\varepsilon]$  with  $\Delta\varepsilon$  is the width of the energy spectrum. When the energy distribution is determined, that is  $P_t(\varepsilon) = 1$ , we have  $S_P(t) = 0$ ,

---


$$\mathcal{L}_n = \lim_{T \rightarrow \infty} \frac{1}{T} \int_0^T L_n(t) dt = \lim_{T \rightarrow \infty} \frac{1}{T} \int_0^T dt \sum_{\alpha, \beta} \langle \psi_n | \alpha \rangle \langle \alpha | \psi_0 \rangle \langle \beta | \psi_n \rangle \langle \psi_0 | \beta \rangle e^{-it(E_\alpha - E_\beta)} = \sum_{\alpha} |\langle \psi_n | \alpha \rangle|^2 |\langle \alpha | \psi_0 \rangle|^2, \quad (13)$$

where  $H_f|\alpha\rangle = E_\alpha|\alpha\rangle$ ,  $H_f|\beta\rangle = E_\beta|\beta\rangle$ , and we have carried out the intergration as the energy spectrum of  $H_f$  is non-degenerate. The  $\mathcal{L}_n$  can be recognized as the overlap between the long time averaged state  $\bar{\rho} = \lim_{T \rightarrow \infty} \int_0^T \rho(t) dt$  and the  $n$ th eigenstate  $\rho_n = |\psi_n\rangle\langle\psi_n|$  of  $H_i$ , so that  $\mathcal{L}_n = \text{Tr}(\bar{\rho}\rho_n)$ . Here, it is worth pointing out that the inverse  $\mathcal{L}_0$  is the participation ratio of the initial state  $|\psi_0\rangle$  with respect to the eigenstates of  $H_f$ .

In Fig. 5(a), we plot the long time averaged Loschmidt echo spectrum  $\mathcal{L}_n$  as a function of  $\delta\kappa$  and  $\varepsilon_n$  for  $\kappa_i = 0.4$  and  $N = 1000$ . We see that the ESQPT at  $\delta\kappa_c = 0.8$  leads to a remarkable change in the behavior of  $\mathcal{L}_n$ , which in turn can be used to diagnose the onset of the ESQPT. Moreover,  $\mathcal{L}_n$  for  $\delta\kappa > \delta\kappa_c$  also shows a dip at the critical energy  $\varepsilon_c$  of the ESQPT, as marked by the horizontal dashed line in the figure.

More informations about the effect of the ESQPT are provided by the energy distribution of the long time averaged state weighted by  $\mathcal{L}_n$ ,

$$P_{\delta\kappa}(\varepsilon) = \sum_n \mathcal{L}_n \delta(\varepsilon - \varepsilon_n). \quad (14)$$

Figs. 5(b)-(e) demonstrate the energy distribution  $P_{\delta\kappa}(\varepsilon)$  for several  $\delta\kappa$  values. One can clearly see that  $P_{\delta\kappa}(\varepsilon)$  exhibits distinct behaviors in different phases of the ESQPT. In particular, as seen in Fig. 5(d), the energy distribution shows a sharp peak at the critical energy of the ESQPT for the critical quench strength, which signals the ESQPT singularity and can be employed to probe the occurrence of the ESQPT.

while  $S_P(t) = \ln \Delta\varepsilon$  implies  $P_t(\varepsilon)$  is uniform, namely  $P_t(\varepsilon) = (\Delta\varepsilon)^{-1}$ .

Fig. 4(b) shows the time evolution of  $S_P(t)$  for the quench strengths that are the same as in Fig. 4(a). We see that the evolutions of  $S_P(t)$  is very similar to the results of  $\Sigma(t)$ , apart from small fluctuations around the saturation value. We also note that  $S_P(t)$  saturates at a very short time scale in comparison with  $\Sigma(t)$ . Moreover, unlike  $\Sigma(t)$  there is no rapid growth in  $S_P(t)$  for the critical quench strength. Nevertheless, the similarity between  $S_P(t)$  and  $\Sigma(t)$  means that both of them can be used to identify the occurrence and different phases of the ESQPT.

## B. Long time averaged Loschmidt echo spectrum

The signatures of the ESQPT are also reflected in the long time averaged Loschmidt echo spectrum, which is calculated as

---

To quantitatively investigate the features of  $P_{\delta\kappa}(\varepsilon)$ , as we have done for the time evolved energy distribution  $P_t(\varepsilon)$ , we study its variation and entropy, which are, respectively, defined by

$$\begin{aligned} \Sigma(\delta\kappa) &= \int d\varepsilon P_{\delta\kappa}(\varepsilon) [\varepsilon - \langle \varepsilon \rangle]^2, \\ S_P(\delta\kappa) &= - \int d\varepsilon P_{\delta\kappa}(\varepsilon) \ln P_{\delta\kappa}(\varepsilon), \end{aligned} \quad (15)$$

where  $\langle \varepsilon \rangle = \int d\varepsilon P_{\delta\kappa}(\varepsilon) \varepsilon$ .

In Fig. 5(f), we display  $\Sigma(\delta\kappa)$  as a function of  $\delta\kappa$  for  $\kappa_i = 0.4$  and  $N = 1000$ . The variation  $\Sigma(\delta\kappa)$  increases with increasing  $\delta\kappa$ , however, it grows in different rate between two phases of the ESQPT. The changing of the growth rate of  $\Sigma(\delta\kappa)$  occurs at the critical quench strength of the ESQPT. As a consequence, the derivative of  $\Sigma(\delta\kappa)$  shows an abrupt decrease and reaches its local minimal value around the critical quench strength. This is seen in the inset of Fig. 5(f), where the derivative of the variation  $\partial_{\delta\kappa}\Sigma$  for different system sizes are plotted. Hence, the variation  $\Sigma(\delta\kappa)$  succinctly captures the signatures of the ESQPT.

The dependence of entropy  $S_P(\delta\kappa)$  on the quench strength is plotted in Fig. 5(g). For  $\delta\kappa < \delta\kappa_c$ ,  $S_P(\delta\kappa)$  grows as  $\delta\kappa$  increases, while it saturates to a stationary value as  $\delta\kappa$  increases for  $\delta\kappa > \delta\kappa_c$ . This difference in the behavior of  $S_P(\delta\kappa)$  allows us to use it to identify different phases of the ESQPT. In the neighborhood of the critical quench strength  $\delta\kappa_c$ , we see a decrease in  $S_P(\delta\kappa)$ . This is more visible in the inset of Fig. 5(f), where we show how

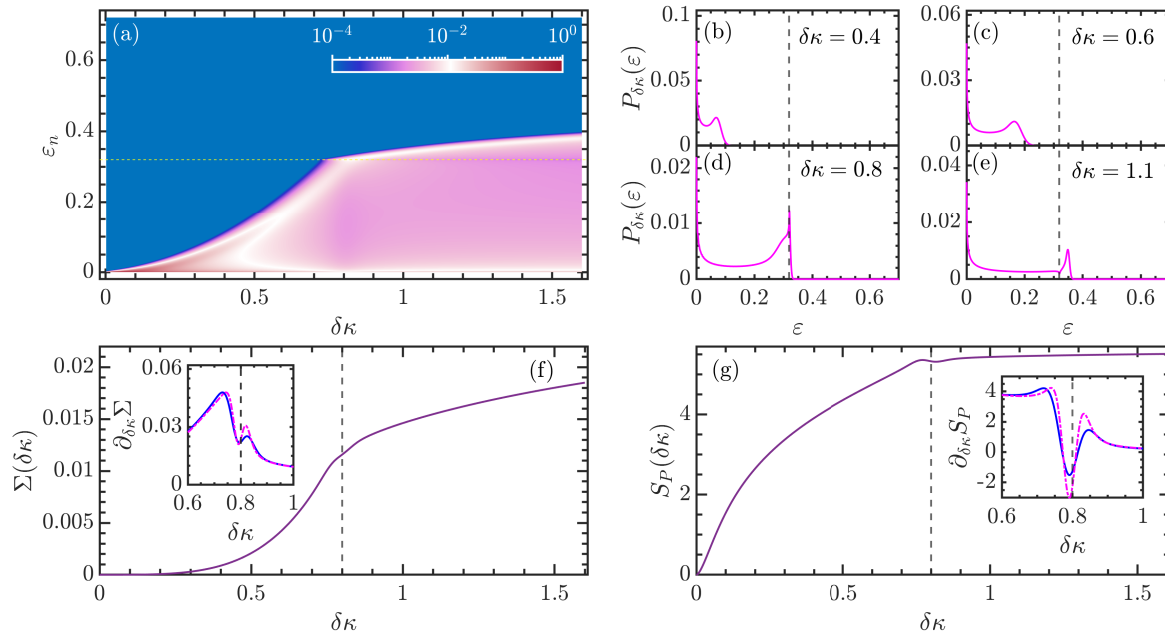


FIG. 5. (a): Heat map of the long time averaged Loschmidt echo spectrum  $\mathcal{L}_n$  as a function of  $\delta\kappa$  and  $\varepsilon_n$  with system size  $N = 1000$ . The horizontal dashed line marks the critical energy  $\varepsilon_c$  of the ESQPT. (b)-(e): Energy distribution of the long time averaged state  $P_{\delta\kappa}(\varepsilon)$  for different values of  $\delta\kappa$  with  $N = 1000$ . The vertical dashed line in each panel denotes the critical energy  $\varepsilon_c$  of the ESQPT, see Eq. (5). (f): Variation of the energy distribution of the long time averaged state as a function of  $\delta\kappa$  for  $N = 1000$ . The inset shows  $\partial_{\delta\kappa}\Sigma$  as a function of  $\delta\kappa$  for  $N = 1000$  (blue solid curve) and  $N = 2000$  (magenta dot-dashed curve). (g): Entropy of the energy distribution of the long time averaged state as a function of  $\delta\kappa$  for  $N = 1000$ . The inset plots  $\partial_{\delta\kappa}S_P$  as a function of  $\delta\kappa$  for  $N = 1000$  (blue solid curve) and  $N = 2000$  (magenta dot-dashed curve). The vertical dashed line in panels (f) and (g) is the critical quench strength  $\delta\kappa_c$ . Other parameters:  $\kappa_i = 0.4$  and  $\delta\kappa_c = 0.8$  obtained from Eq. (8).

the derivative of entropy  $\partial_{\delta\kappa}S_P$  evolves as a function of  $\delta\kappa$  for different system sizes. An obvious dip in the value of  $\partial_{\delta\kappa}S_P$  appears near the critical quench strength, confirming that the entropy  $S_P(\delta\kappa)$  undergoes a decrease as the strength of quench passes through its critical value. Increasing the system size  $N$  tends to sharpen the dip and moving its location to the critical value of  $\delta\kappa$ . The entropy  $S_P(\delta\kappa)$  therefore acts as a witness of the ESQPT.

#### IV. CONCLUSIONS

In summary, by investigating the dynamical signatures of the ESQPT in the spin-1 BEC via the Loschmidt echo spectrum, we have shown the usefulness of the Loschmidt echo spectrum in the studying of ESQPTs in quantum many-body systems. We have explored how the ESQPT gets reflected in the behaviors of the Loschmidt echo spectrum and the associated energy distribution.

The ESQPT in the spin-1 BEC is characterized by the logarithmic divergence of the density of states, which results in the localization of the eigenstates around the ESQPT. A detailed study of the classical limit of the system reveals that the presence of the ESQPT and the corresponding characterizations are a consequence of the saddle point in the classical system.

The analysis of the time evolution of the Loschmidt echo spectrum unveils that the underlying ESQPT leads to a drastic change in the behavior of the Loschmidt echo spectrum. In particular, we see the singular behavior in the evolution of the Loschmidt echo spectrum signals the onset of the ESQPT. We further shown that the occurrence and different phases of the ESQPT are clearly identified in the properties of the energy distribution of the evolved state weighted by the components of the Loschmidt echo spectrum. In addition, an explicit examination of the long time averaged Loschmidt echo and associated energy distribution demonstrates that they can also be utilized to probe the ESQPT.

Although our conclusions are verified for spin-1 BEC, we would expect that qualitatively similar results would be found in other systems that exhibit the logarithmic divergence in their density of states. It would be interesting to explore the relationship between the Loschmidt echo spectrum and the ESQPTs, which are signified by the discontinuity in the derivative of the density of states [3–5]. Finally, our findings extend the usefulness of the Loschmidt echo spectrum in studying of the dynamical quantum phase transitions [75] to ESQPTs, and open a new way to get a better understanding on the dynamical features of ESQPTs.

## ACKNOWLEDGMENTS

This work is supported by the Zhejiang Provincial Nature Science Foundation (Grant Nos. LY20A050001, LQ22A040006); the National Science Foundation of China under grant number 11805165; and the Slovenian Research Agency (ARRS) under grant number J1-4387.

- 
- [1] P. Cejnar, M. Macek, S. Heinze, J. Jolie, and J. Dobeš, *Journal of Physics A: Mathematical and General* **39**, L515 (2006).
- [2] M. Caprio, P. Cejnar, and F. Iachello, *Annals of Physics* **323**, 1106 (2008).
- [3] P. Stránský, M. Macek, and P. Cejnar, *Annals of Physics* **345**, 73 (2014).
- [4] P. Stránský and P. Cejnar, *Physics Letters A* **380**, 2637 (2016).
- [5] P. Cejnar, P. Stránský, M. Macek, and M. Kloc, *Journal of Physics A: Mathematical and Theoretical* **54**, 133028 (2021).
- [6] A. L. Corps and A. Relaño, *Phys. Rev. Lett.* **127**, 130602 (2021).
- [7] S. Sachdev, *Quantum Phase Transitions*, 2nd ed. (Cambridge University Press, 2011).
- [8] F. Pérez-Bernal and F. Iachello, *Phys. Rev. A* **77**, 032115 (2008).
- [9] M. Macek, P. Stránský, A. Leviatan, and P. Cejnar, *Phys. Rev. C* **99**, 064323 (2019).
- [10] W.-T. Dong, Y. Zhang, B.-C. He, F. Pan, Y.-A. Luo, J. P. Draayer, and S. Karampagia, *J. Phys. G: Nucl. Part. Phys.* **48**, 045103 (2021).
- [11] D. Larese, F. Pérez-Bernal, and F. Iachello, *J. Mol. Struct.* **1051**, 310 (2013).
- [12] J. Khalouf-Rivera, F. Pérez-Bernal, and M. Carvajal, *J. Quant. Spectrosc. Radiat. Transfer* **261**, 107436 (2021).
- [13] J. Khalouf-Rivera, M. Carvajal, and F. Pérez-Bernal, *SciPost Phys.* **12**, 2 (2022).
- [14] V. M. Bastidas, P. Pérez-Fernández, M. Vogl, and T. Brandes, *Phys. Rev. Lett.* **112**, 140408 (2014).
- [15] I. García-Mata, E. Vergini, and D. A. Wisniacki, *Phys. Rev. E* **104**, L062202 (2021).
- [16] Q. Wang and F. Pérez-Bernal, *Phys. Rev. E* **104**, 034119 (2021).
- [17] D. Mondal, S. Sinha, and S. Sinha, *Phys. Rev. E* **105**, 014130 (2022).
- [18] Q.-W. Wang and S. Wu, *Phys. Rev. A* **102**, 063531 (2020).
- [19] J. Chávez-Carlos, T. L. M. Lezama, R. G. Cortiñas, J. Venkatraman, M. H. Devoret, V. S. Batista, F. Pérez-Bernal, and L. F. Santos, arXiv e-prints, arXiv:2210.07255 (2022), arXiv:2210.07255 [quant-ph].
- [20] T. Tian, H.-X. Yang, L.-Y. Qiu, H.-Y. Liang, Y.-B. Yang, Y. Xu, and L.-M. Duan, *Phys. Rev. Lett.* **124**, 043001 (2020).
- [21] P. Feldmann, C. Klempt, A. Smerzi, L. Santos, and M. Gessner, *Phys. Rev. Lett.* **126**, 230602 (2021).
- [22] J. Cabedo and A. Celi, *Phys. Rev. Research* **3**, 043215 (2021).
- [23] L. Zhou, J. Kong, Z. Lan, and W. Zhang, arXiv e-prints, arXiv:2209.11415 (2022), arXiv:2209.11415 [cond-mat.quant-gas].
- [24] F. Leyvraz and W. D. Heiss, *Phys. Rev. Lett.* **95**, 050402 (2005).
- [25] M. Šindelka, L. F. Santos, and N. Moiseyev, *Phys. Rev. A* **95**, 010103 (2017).
- [26] D. J. Nader, C. A. González-Rodríguez, and S. Lerma-Hernández, *Phys. Rev. E* **104**, 064116 (2021).
- [27] J. Gamito, J. Khalouf-Rivera, J. M. Arias, P. Pérez-Fernández, and F. Pérez-Bernal, (2022), arXiv:2202.11413 [quant-ph].
- [28] F. Santos and F. Pérez-Bernal, *Phys. Rev. A* **92**, 050101 (2015).
- [29] L. F. Santos, M. Távora, and F. Pérez-Bernal, *Phys. Rev. A* **94**, 012113 (2016).
- [30] P. Pérez-Fernández, P. Cejnar, J. M. Arias, J. Dukelsky, J. E. García-Ramos, and A. Relaño, *Phys. Rev. A* **83**, 033802 (2011).
- [31] T. Brandes, *Phys. Rev. E* **88**, 032133 (2013).
- [32] R. Puebla, A. Relaño, and J. Retamosa, *Phys. Rev. A* **87**, 023819 (2013).
- [33] M. A. Bastarrachea-Magnani, S. Lerma-Hernández, and J. G. Hirsch, *Phys. Rev. A* **89**, 032101 (2014).
- [34] R. Puebla, M.-J. Hwang, and M. B. Plenio, *Phys. Rev. A* **94**, 023835 (2016).
- [35] Q. Wang and F. Pérez-Bernal, *Phys. Rev. E* **103**, 032109 (2021).
- [36] R. Puebla and A. Relaño, *Phys. Rev. E* **92**, 012101 (2015).
- [37] Q. Wang and F. Pérez-Bernal, *Phys. Rev. A* **100**, 022118 (2019).
- [38] Q. Wang and F. Pérez-Bernal, *Phys. Rev. A* **100**, 062113 (2019).
- [39] A. Relaño, J. M. Arias, J. Dukelsky, J. E. García-Ramos, and P. Pérez-Fernández, *Phys. Rev. A* **78**, 060102 (2008).
- [40] P. Pérez-Fernández, A. Relaño, J. M. Arias, J. Dukelsky, and J. E. García-Ramos, *Phys. Rev. A* **80**, 032111 (2009).
- [41] P. Stránský, P. Cejnar, and R. Filip, *Phys. Rev. A* **104**, 053722 (2021).
- [42] M. Kloc, D. Šimsa, F. Hanák, P. R. Kaprálová-Žďánská, P. Stránský, and P. Cejnar, *Phys. Rev. A* **103**, 032213 (2021).
- [43] M. Kloc, P. Stránský, and P. Cejnar, *Phys. Rev. A* **98**, 013836 (2018).
- [44] Q. Hummel, B. Geiger, J. D. Urbina, and K. Richter, *Phys. Rev. Lett.* **123**, 160401 (2019).
- [45] S. Pilatowsky-Cameo, J. Chávez-Carlos, M. A. Bastarrachea-Magnani, P. Stránský, S. Lerma-Hernández, L. F. Santos, and J. G. Hirsch, *Phys. Rev. E* **101**, 010202 (2020).
- [46] A. L. Corps and A. Relaño, *Phys. Rev. A* **105**, 052204 (2022).



- [47] P. Pérez-Fernández, A. Relaño, J. M. Arias, P. Cejnar, J. Dukelsky, and J. E. García-Ramos, *Phys. Rev. E* **83**, 046208 (2011).
- [48] C. M. Lóbez and A. Relaño, *Phys. Rev. E* **94**, 012140 (2016).
- [49] Á. L. Corps, R. A. Molina, and A. Relaño, *J. Phys. A: Math. Theor.* **55**, 084001 (2022).
- [50] Á. L. Corps and A. Relaño, arXiv e-prints, arXiv:2205.03443 (2022), [arXiv:2205.03443 \[cond-mat.stat-mech\]](https://arxiv.org/abs/2205.03443).
- [51] A. L. Corps and A. Relaño, *Phys. Rev. B* **106**, 024311 (2022).
- [52] S. P. Kelly, E. Timmermans, and S.-W. Tsai, *Phys. Rev. A* **102**, 052210 (2020).
- [53] M. R. Lambert, S.-W. Tsai, and S. P. Kelly, *Phys. Rev. A* **106**, 012206 (2022).
- [54] R. Puebla and A. Relaño, *Europhysics Letters* **104**, 50007 (2014).
- [55] B. Dietz, F. Iachello, M. Miski-Oglu, N. Pietralla, A. Richter, L. von Smekal, and J. Wambach, *Phys. Rev. B* **88**, 104101 (2013).
- [56] Y. Kawaguchi and M. Ueda, *Physics Reports* **520**, 253 (2012).
- [57] D. M. Stamper-Kurn and M. Ueda, *Rev. Mod. Phys.* **85**, 1191 (2013).
- [58] J. Stenger, S. Inouye, D. M. Stamper-Kurn, H.-J. Miesner, A. P. Chikkatur, and W. Ketterle, *Nature* **396**, 345 (1998).
- [59] L. E. Sadler, J. M. Higbie, S. R. Leslie, M. Vengalattore, and D. M. Stamper-Kurn, *Nature* **443**, 312 (2006).
- [60] F. Gerbier, A. Widera, S. Fölling, O. Mandel, and I. Bloch, *Phys. Rev. A* **73**, 041602 (2006).
- [61] C. D. Hamley, C. S. Gerving, T. M. Hoang, E. M. Bookjans, and M. S. Chapman, *Nature Physics* **8**, 305 (2012).
- [62] L. Zhao, J. Jiang, T. Tang, M. Webb, and Y. Liu, *Phys. Rev. A* **89**, 023608 (2014).
- [63] X.-Y. Luo, Y.-Q. Zou, L.-N. Wu, Q. Liu, M.-F. Han, M. K. Tey, and L. You, *Science* **355**, 620 (2017), <https://www.science.org/doi/pdf/10.1126/science.aag1106>.
- [64] C. B. Dağ, S.-T. Wang, and L.-M. Duan, *Phys. Rev. A* **97**, 023603 (2018).
- [65] W. Zhang, S. Yi, and L. You, *New Journal of Physics* **5**, 77 (2003).
- [66] Z. Zhang and L.-M. Duan, *Phys. Rev. Lett.* **111**, 180401 (2013).
- [67] M. Xue, S. Yin, and L. You, *Phys. Rev. A* **98**, 013619 (2018).
- [68] D. Jacob, L. Shao, V. Corre, T. Zibold, L. De Sarlo, E. Mimoun, J. Dalibard, and F. Gerbier, *Phys. Rev. A* **86**, 061601 (2012).
- [69] M. Anquez, B. A. Robbins, H. M. Bharath, M. Boguslawski, T. M. Hoang, and M. S. Chapman, *Phys. Rev. Lett.* **116**, 155301 (2016).
- [70] Y. Liu, S. Jung, S. E. Maxwell, L. D. Turner, E. Tiesinga, and P. D. Lett, *Phys. Rev. Lett.* **102**, 125301 (2009).
- [71] E. M. Bookjans, A. Vinit, and C. Raman, *Phys. Rev. Lett.* **107**, 195306 (2011).
- [72] J. Jiang, L. Zhao, M. Webb, and Y. Liu, *Phys. Rev. A* **90**, 023610 (2014).
- [73] A. Vinit and C. Raman, *Phys. Rev. A* **95**, 011603 (2017).
- [74] H.-Y. Liang, L.-Y. Qiu, Y.-B. Yang, H.-X. Yang, T. Tian, Y. Xu, and L.-M. Duan, *New Journal of Physics* **23**, 033038 (2021).
- [75] C. Y. Wong and W. C. Yu, *Phys. Rev. B* **105**, 174307 (2022).
- [76] M. Rautenberg and M. Gärttner, *Phys. Rev. A* **101**, 053604 (2020).
- [77] W. Zhang, D. L. Zhou, M.-S. Chang, M. S. Chapman, and L. You, *Phys. Rev. A* **72**, 013602 (2005).
- [78] M. C. Gutzwiller, *Chaos in classical and quantum mechanics*, Vol. 1 (Springer Science & Business Media, 2013).
- [79] K. Husimi, *Proc. Phys. Math. Soc. Jpn* **22**, 264 (1940).
- [80] Q. Wang and H. T. Quan, *Phys. Rev. E* **96**, 032142 (2017).
- [81] S. Pappalardi, A. Russomanno, B. Žunkovič, F. Iemini, A. Silva, and R. Fazio, *Phys. Rev. B* **98**, 134303 (2018).
- [82] T. Xu, T. Scaffidi, and X. Cao, *Phys. Rev. Lett.* **124**, 140602 (2020).
- [83] K. Hashimoto, K.-B. Huh, K.-Y. Kim, and R. Watanabe, *Journal of High Energy Physics* **2020**, 68 (2020).
- [84] R. A. Kidd, A. Safavi-Naini, and J. F. Corney, *Phys. Rev. A* **103**, 033304 (2021).